HHS Public Access

Author manuscript

Mol Imaging. Author manuscript; available in PMC 2015 October 29.

Published in final edited form as:

Mol Imaging. 2015 September 1; 14: 516–525.

Determination of Fatty Acid Metabolism with Dynamic ^{11}C-Palmitate Positron Emission Tomography of Mouse Heart *In Vivo*

Yinlin Li[1,4], **Tao Huang**[1], **Xinyue Zhang**[4], **Min Zhong**[1], **Natalie N. Walker**[2], **Jiang He**[1], **Stuart S. Berr**[1], **Susanna R. Keller**[2], and **Bijoy K. Kundu**[1,3,*]

[1]Department of Radiology and Medical Imaging, University of Virginia, Charlottesville, VA, USA.

[2]Department of Medicine, Division of Endocrinology and Metabolism, University of Virginia, VA, USA.

[3]Cardiovascular Research Center, University of Virginia, Charlottesville, VA, USA.

[4]School of Mechatronic Engineering, Beijing Institute of Technology, Beijing, China

Abstract

The goal of this study was to establish a quantitative method for measuring FA metabolism with partial volume (PV) and spill-over (SP) corrections using dynamic ^{11}C-palmitate PET images of mouse heart *in vivo*.

Methods—Twenty-minute dynamic ^{11}C-palmitate PET scans of four 18–20 week old male C57BL/6 mice under isoflurane anesthesia were performed using a Focus 120 PET scanner. A model corrected blood input function (MCIF), by which the input function with SP and PV corrections and the metabolic rate constants (k_1−k_5) are simultaneously estimated from the dynamic ^{11}C-palmitate PET images of mouse hearts in a 4-compartment tracer kinetic model, was used to determine rates of myocardial FA oxidation (MFAO), myocardial FA esterification (MFAE), myocardial FA utilization (MFAU) and myocardial FA uptake (MFAUp).

Results—The MFAO thus measured in C57BL/6 mice was 375.03±43.83 nmoles/min/g. This compares well with the MFAO measured in perfused working C57BL/6 mouse hearts *ex vivo* of about 350 nmoles/g/min and 400 nmoles/min/g.

Conclusions—FA metabolism was measured for the first time in mouse heart *in vivo* using dynamic ^{11}C-palmitate PET in a 4-compartment tracer kinetic model. MFAO obtained with this model were validated by results previously obtained with mouse hearts *ex vivo*.

Keywords

^{11}C-palmitate PET; Fatty-acid Metabolism in Heart; 4-Compartment Tracer Kinetic Model; Spill-over; Partial Volume Corrections

[*]**Corresponding Author:** Bijoy K. Kundu, PhD, Assistant Professor, Department of Radiology and Medical Imaging, Cardiovascular Research Center, University of Virginia, Charlottesville, VA 22908, bkk5a@virginia.edu, Phone: 434-924-0284, Fax: 434-924-9435.

CONFLICT OF INTEREST

The authors declare that they have no conflict of interest.

INTRODUCTION

Heart failure (HF) affects nearly 6 million people in the United States. Coronary heart disease, high blood pressure, and diabetes are common causes of HF. The estimated cost for HF management in the US is about 34 billion dollars per year [1]. Current medical therapies are ineffective with a five year survival rate of only 25% [2]. It is well established that cardiac metabolism is inextricably linked to cardiac function and modulation of substrate energy metabolism may be an attractive strategy for treatment of HF [3–5]. However, the molecular mechanisms connecting cardiac function and metabolism are not well understood and our current understanding of metabolic alterations in the heart is largely based on *ex vivo* studies in animal models [6–9]. Transgenic and knockout mouse models offer opportunities to address this issue *in vivo* and in parallel at the molecular level. However, a severe limitation to this approach is that there are no suitable methods that allow non-invasive assessment of cardiac energy metabolism and correlation to cardiac function in an intact mouse.

Imaging myocardial metabolism in mouse heart is challenging due to the limited intrinsic resolution of small animal scanners and the small size of the mouse heart, resulting in image blur. Recently, we have optimized a model corrected blood input function from time-resolved gated 2-[^{18}F] fluoro-2-deoxy-D-glucose (FDG) PET images of mouse heart to measure myocardial glucose metabolism *in vivo*[10,11]. Measuring FA metabolism using ^{11}C-palmitate in mouse heart is even more challenging than measuring glucose metabolism due to the long range of positrons emitted by ^{11}C. Poor quality of images results in severe partial volume (PV) averaging and spill-over (SP) contamination is further confounded by the rapid heart rate. Previous studies using ^{11}C-palmitate PET have only been performed in dog and rat hearts [12–15]. In this study we developed a method to measure FA metabolism from dynamic ^{11}C-palmitate PET images of mouse heart using a 4-compartment tracer kinetic model, for the first time, *in vivo*. Our computed rate of myocardial FA oxidation in mouse heart *in vivo* was in agreement with the measured palmitate oxidation in the working mouse heart *ex vivo*[16].

MATERIALS AND METHODS

Animal Model

Four adult C57BL/6N male mice (18–20 weeks of age) were imaged using the Focus-F120 PET scanner (Siemens Medical Solutions USA, Inc., Malvern, PA) under isoflurane anesthesia [17]. The mice were kept on a normal chow diet (7912 Teklad LM-485 from Harlan Laboratories) and had free access to food and water before the study. All experiments were performed in compliance with the Guide for the Care and Use of Laboratory Animals, published by the National Institutes of Health and was conducted under protocols approved by the Institutional Animal Care and Use Committee at the University of Virginia.

^{11}C-palmitate labeling

^{11}C-Palmitate radiolabeling was performed in the Radiochemistry Core Laboratory at the University of Virginia Molecular Imaging Center using the Modular-Lab PharmTracer system (Eckert & Ziegler, E&Z, Hopkinton, MA). We modified the E&Z cassette and software designed for the production of ^{11}C-acetate in order to make ^{11}C-palmitate following the method of Mock et al [18]. Briefly, ^{11}C-CO_2 from the cyclotron was trapped by carbospheres at −20°C in order to remove excess helium carrier gas. The carbospheres were heated to 60°C at which point helium was passed over the carbospheres to force the ^{11}C-CO_2 through the precursor solutions which consisted of 0.143M pentadecylmagnesium bromide in diethyl ether (NOVEL Chemical Solutions, Crete, NE). The reaction vessel was then sealed and heated to 30°C for 3 minutes to complete the reaction. The reaction was quenched with 1 Normal HCl diethyl ether. The quenched solution was passed through a dry Alumina-N Sep-Pak Plus cartridge that trapped the polar ^{11}C-palmitic acid. Nonpolar chemicals were removed from the Sep-Pak by rinsing with three 1-ml diethyl ether washes. The Sep-Pak was rinsed with two 1-ml portions of 0.5 M NaH_2PO_4 solution to disrupt the carboxylic acid binding to the alumina surface, followed by two 1-ml water washes to remove soluble Mg^{2+} salts from the Sep-Pak. The ^{11}C-palmitic acid was eluted from the Sep-Pak with 3 portions of absolute ethanol (2 ml total volume) and the solution was then passed through a sterile 0.2-μm Millex-FG filter (EMD Millipore, Darmstadt, Germany) into a sterile intermediate product vial. The non-decay-corrected radiochemical yield of the ^{11}C-palmitic acid product averaged ~30% (250 mCi of ^{11}C-CO_2 yielded 75 mCi of ^{11}C-palmitate). The ^{11}C-palmitate ethanol solution was formulated with bovine serum albumin. The synthesis was completed within about 30 minutes.

PET Imaging

Using the ^{11}C-palmitate label described above, we imaged FA metabolism in mouse heart *in vivo* as following. Briefly, a mouse with ECG surface electrodes and a respiratory pillow attached to its limbs and chest, respectively, and under 1–1.5% isoflurane anesthesia was positioned in the bore of the PET scanner [19]. A 10 minute Co-57 transmission scan was performed for attenuation correction. A 20 minute dynamic PET acquisition was then initiated prior to the administration of 300–350 μCi in about 200–300 μl of ^{11}C-palmitate via tail-vein over 30 seconds. The list-mode dynamic PET data was reconstructed using OSEM-MAP algorithm [20] with attenuation correction into the following dynamic frames (frames, time(s):12,5;8,30;4,150;1,300). The reconstructed images were composed of 95 transverse slices with a thickness of 0.79 mm and an in-plane voxel resolution of 0.4 × 0.4 mm (128×128 pixels) corresponding to a zoom factor of 2.13. Regions of interest in the region corresponding to the LV blood pool (LVBP) and the myocardium were drawn in the last time frame of the dynamic image data in the transverse plane and time activity curves generated for the LVBP and the myocardium for the 20 minute scan. The blood and the myocardium time activity curves were used in a 4-compartment tracer kinetic model (described below), written in MATLAB (The Mathworks, Natick, MA) using non-linear regression with SP and PV corrections, to compute myocardial FA metabolism including FA oxidation, esterification, utilization and uptake in mouse heart *in vivo*.

4-Compartment Tracer Kinetic Model

Following Bergmann et al [15], the differential equations for ^{11}C-palmitate kinetics can be written as follows:

$$\frac{\partial q_1}{\partial t} = F\left[C_a(t) - \frac{q_1}{V}\right] + k_2 q_2 - k_1 q_1 \quad \text{Eq.1}$$

$$\frac{\partial q_2}{\partial t} = k_1 q_1 + k_4 q_3 - (k_2 + k_3 + k_5) q_2 \quad \text{Eq.2}$$

$$\frac{\partial q_3}{\partial t} = k_3 q_2 - k_4 q_3 \quad \text{Eq.3}$$

$$\frac{\partial q_4}{\partial t} = k_5 q_2 - \frac{F}{V} q_4 \quad \text{Eq.4}$$

where, $q_1 - q_4$ are the concentrations in the 4 compartments as shown in Figure 1. *kn* represents the turnover rate constants between the compartments, *F* is myocardial blood flow and *V* is the vascular volume. *Ca (t)* is the arterial concentration of tracer over time.

The total tracer concentration in myocardium can be defined by the sum of the tracer in each compartment:

$$C_T(t) = q_1(t) + q_2(t) + q_3(t) + q_4(t) \quad \text{Eq.5}$$

Performing Laplace and Inverse Laplace transforms (see Supplementary Material), we get the final form as:

$$C_T(t) = q_1(t) + q_2(t) + q_3(t) + q_4(t) = F \cdot M \otimes C_a(t) \quad \text{Eq.6}$$

where *M* is composed of the rate constants $(k_1 - k_5)$ and *F/V*.

Dual Output Model

Ideally, when a region of interest is drawn within the cavity of the left ventricle, the image derived input function (IDIF) would equal the whole-blood time activity curve *Ca(t)*. However, due to SP and PV effects, the model equation for an image-derived time activity curve from the blood pool can be written as fractions of the tissue concentration in the blood compartment and partial recovery of radio activity concentration from the blood as:

$$Model_{IDIF,i} = \frac{\int_{t_b^i}^{t_e^i} [S_{mb} C_T(t) + r_b C_a(t)]\, dt}{t_e^i - t_b^i} \quad \text{Eq.7}$$

Similarly, the myocardium tissue of the model equation is:

$$Model_{myo,i}=\frac{\int_{t_b^i}^{t_e^i}[r_m C_T(t)+S_{bm}C_a(t)]\,dt}{t_e^i-t_b^i} \quad \text{Eq.8}$$

where, r_b and r_m are the recovery coefficients (accounting for PV effect) for the myocardium and blood pool respectively. S_{mb} and S_{bm} are the SP coefficients from the blood pool to the myocardium and vice versa respectively. t_e^i and t_b^i are the beginning and end times respectively for frame in a dynamic PET scan.

The model equation for the blood input function can be written as:

$$C_a(t)=(A_1(t-\tau)-A_2-A_3)e^{L_1(t-\tau)}+A_2e^{L_2(t-\tau)}+A_3e^{L_3(t-\tau)} \quad \text{Eq.9}$$

where, each of the terms determines the amplitude, shape and wash-out of the tracer over time. ι indicates the time lag between the initiation of imaging and injection of the tracer. The model equations can be fitted to the blood (PET_{IDIF}) and myocardial tissue (PET_{myo}) time-activity curves obtained from OSEM-MAP dynamic PET images with attenuation correction by substituting Eq.6 and Eq. 9 in Eq. 7 and Eq. 8, as indicated below:

$$\mathrm{O(p)}=\sum_{n}^{i=1}\left[(Model_{IDIF,i}-PET_{IDIF,i})^2+(Model_{myo,i}-PET_{myo,i})^2\right] \quad \text{Eq.10}$$

Interpolation and simultaneous estimation

The shorter reconstructed frames at the early time points limited the data resolution, resulting in fluctuations in the blood and tissue time activity curves at these points. A cubic spline interpolation was used to approximate the peak of curve and improve the accuracy of fitting. The interpolation was used near the peak ($PET_{IDIF,max}$, $PET_{myo,max}$) of blood ($PET_{IDIF,i}$) and tissue ($PET_{myo,i}$) concentrations obtained from the dynamic PET data. The interpolated sequences were written as:

$PET_{IDIF,i}$ = [$PET_{IDIF,1}$,……, $PET_{IDIF,max-1}$, PET_{IDIF,k_1},……, PET_{IDIF,k_n}, $PET_{IDIF,max}$, $PET_{IDIF,k_{n+1}}$, ……, $PET_{IDIF,k_{2n}}$, $PET_{IDIF,max+1}$,……];

$PET_{myo,i}$ = [$PET_{myo,1}$,……, $PET_{myo,max-1}$, PET_{myo,k_1},……, PET_{myo,k_n}, $PET_{myo,max}$, $PET_{myo,k_{n+1}}$, ……, $PET_{myo,k_{2n}}$, $PET_{myo,max+1}$,……].

All numeric analyses were done using MATLAB R2013b (The Mathworks, Natick, MA). The optimization was performed by minimizing the objective function (Eq.10) using the MATLAB function “fmincon”, which is based on an interior-reflective Newton method. The initial guesses and bounds for all the parameters used in the optimization routine are shown in Table 1.

The following constraints and prior knowledge were used to set the bounds: a) rates of palmitate oxidation are greater than esterification i.e. $k_5 > k_3$ under control conditions [15]; b) in the steady state, the rate of back flow from compartment 3 (neutral lipids and amino acids) to 2 (interstitial and cytosolic) is close to zero i.e. $k_4=0$ [15] and c) the bounds for the recovery coefficients were based on structural measurements using MRI of control mouse

heart [21]. Since the spill-over factors, S_{bm} and S_{mb}, are changing with time (multiplied with time dependent image-derived blood and tissue curves, Eqs 7 and 8), there is no good way to get a prior estimate of these factors. Hence, we set the bounds for these factors from 0 to 1. We also observed that the computed results have little influence on the changes in the bounds and initial guess values of the 7-parameter blood function (Eq 9).

The minimization of Eq.10 results in simultaneous estimation of the parameters of blood input function *Ca (t)*, compartment model parameters k_1-k_5 and the SP and PV coefficients (S_{mb},r_b,r_m,S_{bm}). The optimized rate constants and *SP* and *PV* coefficients are listed in Table 2. A myocardial blood flow (F) value of 4.8 ml/min/g [22] and vascular blood volume (V) of 0.1 ml/g [15] was used for the calculations.

Free Fatty Acid (FFA) in mouse blood

For the measurement of FFA levels in the mouse blood, samples (~20 ul) from the tail vein were collected during the dynamic PET scan at 10 and 15 minutes post tracer administration, using non-heparinized capillary tubes. The blood was allowed to clot for 30 minutes, serum was then separated from the clot by centrifugation (15 min at 1600 g at room temperature in a microcentrifuge) and stored in a −20° C freezer until analyzed. FFA levels were measured using HR series NEFA-HR2 reagents (Wako Life Sciences Inc., Richmond, VA).

RESULTS

In this study, using dynamic ^{11}C-palmitate PET of mouse heart *in vivo*, we have measured myocardial FA metabolism including rates of oxidation, esterification, utilization and uptake. Figure 2A shows an example of a ^{11}C-palmitate PET image of mouse heart *in vivo*. Regions of interest (ROI) are shown in the blood and the myocardium in the last time frame. The ROI drawn in the last time frame was used to obtain time activity curves (TACs) for the blood and the myocardium from the dynamic PET data. In Figure 2B, the model fits (Eqs 7–10) to the blood and myocardium TACs are shown without interpolation resulting in poor fit to the blood TAC around the peak region. Cubic spline interpolation with a time interval of 0.5 s around the peak resulted in better fits to both the blood and myocardium TACs (Figure 2C). Model fits resulted in simultaneous estimation of blood input function *Ca (t)*, compartment model parameters k_1-k_5 and the SP and PV coefficients (S_{mb},r_b,r_m,S_{bm}). The model corrected blood input function (MCIF), *Ca(t)*, was compared to the image-derived blood input function (PET blood) in Figure 3. The recovery coefficients for the blood pool and the myocardium are denoted by r_b and r_m respectively. Since they are a function of structure, the bounds used in the optimization routine were based on structural measurements using MRI of control mouse heart [21]. As indicated in Figure 3, the model correction results in a ~20% increase in the model corrected input function (MCIF) at the early time points compared to image-derived input function (PET blood) indicating improved radioactivity recovery. Model correction also eliminated SP contamination from the myocardium into the blood pool at the late time points.

Using the formulas described in detail in Supplementary Material, under steady state condition, the rates of myocardial FA oxidation (MFAO), esterification (MFAE) and hence utilization (MFAU) were computed. Figure 4 shows the computed average MFAO

(375.03±43.83 nmoles/g/min), MFAE (10.97 ±7.11 nmoles/g/min) and MFAU (385.99 ±49.51nmoles/g/min) obtained by optimization of the dynamic ^{11}C-palmitate PET data from four 18–20 week old male C57BL/6N mice. The above computed MFAO *in vivo* agrees with the range of MFAO measured *ex vivo* in perfused working 12 and 15 week old strain-matched mouse heart [16].

Myocardial FA uptake rate (MFAUp) was also computed by dividing MFAU with measured FFA (849 nM/mL) in mouse blood. The computed MFAUp rate was 0.45±0.06 ml/min/g. When compared with the rate of myocardial FDG uptake, Ki (0.15±0.03 ml/min/g) measured in age- and strain-matched mice in a previously published study from our laboratory [10], we observed a 3-fold higher uptake rate of palmitate (MFAUp) compared to FDG uptake rate, Ki.

DISCUSSION

The commonly used tracers for measuring myocardial FA metabolism are 14(R,S)-[18F]fluoro-6-thia-heptadecanoic acid (FTHA)[23] and ^{11}C-palmitate [12,24]. There is a distinct advantage in using ^{11}C-palmitate due to the short half-life of the labeled tracer allowing serial measurements of FA and glucose metabolism in the same animal and monitoring the effect of therapy *in vivo*. Imaging the mouse heart using a small animal PET scanner is a challenge due to the limited intrinsic resolution [19] caused primarily by the finite positron range, which results in image blur. This leads to incomplete radioactivity recovery (PV averaging) and hence SP of radioactivity from the myocardium to the blood pool (BP) and vice versa. Cardiac motion results in further image blur confounding the effects of SP contamination in the image-derived blood input function [25]. In a recent study we optimized a model corrected blood input function (MCBIF) from time-resolved gated FDG PET images of mouse heart *in vivo*[10]. The MCBIF was then used to evaluate glucose metabolism in the pressure overload mouse heart *in vivo*[11]. We observed that under transverse aortic constriction (TAC) induced pressure overload stress, the mouse heart exhibited a 6-fold increase in FDG uptake at day 1 post-TAC with preserved contractile function indicating an adaptive metabolic response. At day 7 post-TAC a further increase in myocardial FDG uptake was found together with a decrease in cardiac function indicating maladaptation [11]. However, how changes in FA metabolism relate to cardiac dysfunction in the stressed mouse heart is not known.

Clinical data using ^{11}C-palmitate PET in hypertensive left ventricular hypertrophy (LVH) suggested a decrease in myocardial FA oxidation and utilization as possible causes for a decrease in myocardial efficiency [26]. Recent ^{18}F-FTHA PET imaging studies *in vivo* in the spontaneously hypertensive rat (SHR) heart over a period of 20 months observed a significant increase in both glucose and fatty acid utilization, which appeared to precede mechanical changes in LVH progression [27]. Studies in a Dahl salt-sensitive rat model *ex vivo*, however, showed the decrease in fatty acid metabolism to occur late in the progression from LVH to heart failure, while glucose uptake was increased at an earlier stage [28]. These studies indicate that there is no clear consensus yet on the abnormalities in fatty acid metabolism in the stressed heart. Improved tools for quantitatively imaging fatty acid

metabolism in a compartment model are needed to complement the conventional graphical Patlak analysis [27].

In this study we optimized and implemented a 4-compartment tracer kinetic model with SP and PV corrections to quantify FA metabolism from dynamic ^{11}C-palmitate images of mouse heart *in vivo*. We measured rates of myocardial fatty acid oxidation (MFAO), esterification (MFAE), utilization (MFAU) and uptake (MFAUp) for the first time in mouse heart *in vivo*. This method can be easily implemented to evaluate the role of FA metabolism in the pressure overload mouse heart *in vivo*.

Our study, however, is not without limitations. The blood input curves obtained from dynamic PET images were not corrected for the conversion of palmitate to $^{11}CO_2$. But studies in dog hearts have shown that this correction performed by arterial blood sampling only modestly affects the input curve especially in the tail region [15]. The factors that may be affected as a result are k_3 (rate of transfer to triglycerides) and the fractional esterification rates since they are represented by the tail of the time activity curve. Our data in mouse heart however suggests that the tail of the input curve may be minimally affected by the correction due to the conversion of palmitate to $^{11}CO_2$. Thus, this correction may not be necessary when imaging a mouse heart using ^{11}C-palmitate, making the process of obtaining the FA metabolic parameters completely non-invasive.

CONCLUSIONS

We have measured FA metabolism including myocardial fatty acid oxidation, esterification, utilization and uptake for the first time from dynamic ^{11}C-palmitate PET images of mouse heart *in vivo*. The results for MFAO measured *in vivo* compared well to the measured range of palmitate oxidation from perfused working mouse heart *ex vivo*. By comparing rates of FA uptake measured in this study with rates of FDG uptake determined in an earlier study, we corroborate that the normal mouse heart preferentially utilizes FA over glucose.

Supplementary Material

Refer to Web version on PubMed Central for supplementary material.

ACKNOWLEDGEMENTS

This work was supported in part by grants from the National Institutes of Health R21 HL-102627 (to B.K.K) and R01 DK-81471(to S.R.K.). We thank Gina Wimer and Jeremy Gatesman for performing the tail vein injections during the course of the study.

References

1. Heidenreich PA, Trogdon JG, Khavjou OA, Butler J, Dracup K, Ezekowitz MD, Finkelstein EA, Hong Y, Johnston SC, Khera A, Lloyd-Jones DM, Nelson SA, Nichol G, Orenstein D, Wilson PW, Woo YJ. Forecasting the future of cardiovascular disease in the United States: a policy statement from the American Heart Association. Circulation. 2011; 123:933–944. [PubMed: 21262990]
2. Ammar KA, Jacobsen SJ, Mahoney DW, Kors JA, Redfield MM, Burnett JC Jr, Rodeheffer RJ. Prevalence and prognostic significance of heart failure stages: application of the American College of Cardiology/American Heart Association heart failure staging criteria in the community. Circulation. 2007; 115:1563–1570. [PubMed: 17353436]

3. Taegtmeyer H. Cardiac Metabolism as a Target for the Treatment of Heart Failure. Circulation. 2004; 110:894–896. [PubMed: 15326079]

4. Lopaschuk GD. Optimizing cardiac fatty acid and glucose metabolism as an approach to treating heart failure. Semin Cardiothorac Vasc Anesth. 2006; 10:228–230. [PubMed: 16959756]

5. Turer AT, Malloy CR, Newgard CB, Podgoreanu MV. Energetics and metabolism in the failing heart: important but poorly understood. Curr Opin Clin Nutr Metab Care. 2010; 13:458–465. [PubMed: 20453645]

6. Doenst T, Pytel G, Schrepper A, Amorim P, Farber G, Shingu Y, Mohr FW, Schwarzer M. Decreased rates of substrate oxidation ex vivo predict the onset of heart failure and contractile dysfunction in rats with pressure overload. Cardiovasc Res. 2010; 86:461–470. [PubMed: 20035032]

7. Taegtmeyer H, Overturf ML. Effects of moderate hypertension on cardiac function and metabolism in the rabbit. Hypertension. 1988; 11:416–426. [PubMed: 3366475]

8. Goodwin GW, Taylor CS, Taegtmeyer H. Regulation of energy metabolism of the heart during acute increase in heart work. J Biol Chem. 1998; 273:29530–29539. [PubMed: 9792661]

9. Taegtmeyer H, Hems R, Krebs HA. Utilization of energy-providing substrates in the isolated working rat heart. Biochem J. 1980; 186:701–711. [PubMed: 6994712]

10. Zhong M, Kundu BK. Optimization of a Model Corrected Blood Input Function From Dynamic FDG-PET Images of Small Animal Heart In Vivo. IEEE Trans Nucl Sci. 2013; 60:3417–3422. [PubMed: 24741130]

11. Zhong M, Alonso CE, Taegtmeyer H, Kundu BK. Quantitative PET Imaging Detects Early Metabolic Remodeling in a Mouse Model of Pressure-Overload Left Ventricular Hypertrophy In Vivo. J Nucl Med. 2013; 54:609–615. [PubMed: 23426760]

12. Welch MJ, Lewis JS, Kim J, Sharp TL, Dence CS, Gropler RJ, Herrero P. Assessment of myocardial metabolism in diabetic rats using small-animal PET: a feasibility study. J Nucl Med. 2006; 47:689–697. [PubMed: 16595504]

13. Shoghi KI, Gropler RJ, Sharp T, Herrero P, Fettig N, Su Y, Mitra MS, Kovacs A, Finck BN, Welch MJ. Time course of alterations in myocardial glucose utilization in the Zucker diabetic fatty rat with correlation to gene expression of glucose transporters: a small-animal PET investigation. J Nucl Med. 2008; 49:1320–1327. [PubMed: 18632819]

14. Shoghi KI, Finck BN, Schechtman KB, Sharp T, Herrero P, Gropler RJ, Welch MJ. In vivo metabolic phenotyping of myocardial substrate metabolism in rodents: differential efficacy of metformin and rosiglitazone monotherapy. Circ Cardiovasc Imaging. 2009; 2:373–381. [PubMed: 19808625]

15. Bergmann SR, Weinheimer CJ, Markham J, Herrero P. Quantitation of myocardial fatty acid metabolism using PET. J Nucl Med. 1996; 37:1723–1730. [PubMed: 8862319]

16. Wright JJ, Kim J, Buchanan J, Boudina S, Sena S, Bakirtzi K, Ilkun O, Theobald HA, Cooksey RC, Kandror KV, Abel ED. Mechanisms for increased myocardial fatty acid utilization following short-term high-fat feeding. Cardiovasc Res. 2009; 82:351–360. [PubMed: 19147655]

17. Flores JE, McFarland LM, Vanderbilt A, Ogasawara AK, Williams SP. The effects of anesthetic agent and carrier gas on blood glucose and tissue uptake in mice undergoing dynamic FDG-PET imaging: sevoflurane and isoflurane compared in air and in oxygen. Mol Imaging Biol. 2008; 10:192–200. [PubMed: 18516648]

18. Mock BH, Brown-Proctor C, Green MA, Steele B, Glick-Wilson BE, Zheng QH. An automated SPE-based high-yield synthesis of [11C]acetate and [11C]palmitate: no liquid-liquid extraction, solvent evaporation or distillation required. Nucl Med Biol. 2011; 38:1135–1142. [PubMed: 21831651]

19. Tai YC, Ruangma A, Rowland D, Siegel S, Newport DF, Chow PL, Laforest R. Performance evaluation of the microPET focus: a third-generation microPET scanner dedicated to animal imaging. J Nucl Med. 2005; 46:455–463. [PubMed: 15750159]

20. Qi JY, Leahy RM, Cherry SR, Chatziioannou A, Farquhar TH. High-resolution 3D Bayesian image reconstruction using the microPET small-animal scanner. Physics in Medicine and Biology. 1998; 43:1001–1013. [PubMed: 9572523]

21. Locke LW, Berr SS, Kundu BK. Image-Derived Input Function from Cardiac Gated Maximum a Posteriori Reconstructed PET Images in Mice. Mol Imaging Biol. 2011; 13:342–347. [PubMed: 20521133]

22. Zhong M, Mistry M, Dimastromatteo J, Taegtmeyer H, Glover DK, Kundu BK. PET Imaging of Myocardial Blood Flow in the Stressed Mouse Heart in vivo, [Abstract]. J. Nucl. Med. 2013; 54:1635.

23. Takala TO, Nuutila P, Pulkki K, Oikonen V, Gronroos T, Savunen T, Vahasilta T, Luotolahti M, Kallajoki M, Bergman J, Forsback S, Knuuti J. 14(R,S)-[18F]Fluoro-6-thia-heptadecanoic acid as a tracer of free fatty acid uptake and oxidation in myocardium and skeletal muscle. Eur J Nucl Med Mol Imaging. 2002; 29:1617–1622. [PubMed: 12458396]

24. de las Fuentes L, Herrero P, Peterson LR, Kelly DP, Gropler RJ, vila-Roman VG. Myocardial fatty acid metabolism: independent predictor of left ventricular mass in hypertensive heart disease. Hypertension. 2003; 41:83–87. [PubMed: 12511534]

25. Laforest R, Sharp TL, Engelbach JA, Fettig NM, Herrero P, Kim J, Lewis JS, Rowland DJ, Tai YC, Welch MJ. Measurement of input functions in rodents: challenges and solutions. Nucl Med Biol. 2005; 32:679–685. [PubMed: 16243642]

26. de las Fuentes L, Soto PF, Cupps BP, Pasque MK, Herrero P, Gropler RJ, Waggoner AD, vila-Roman VG. Hypertensive left ventricular hypertrophy is associated with abnormal myocardial fatty acid metabolism and myocardial efficiency. J Nucl Cardiol. 2006; 13:369–377. [PubMed: 16750782]

27. Hernandez AM, Huber JS, Murphy ST, Janabi M, Zeng GL, Brennan KM, O'Neil JP, Seo Y, Gullberg GT. Longitudinal evaluation of left ventricular substrate metabolism, perfusion, and dysfunction in the spontaneously hypertensive rat model of hypertrophy using small-animal PET/CT imaging. J Nucl Med. 2013; 54:1938–1945. [PubMed: 24092939]

28. Kato T, Niizuma S, Inuzuka Y, Kawashima T, Okuda J, Tamaki Y, Iwanaga Y, Narazaki M, Matsuda T, Soga T, Kita T, Kimura T, Shioi T. Analysis of metabolic remodeling in compensated left ventricular hypertrophy and heart failure. Circ Heart Fail. 2010; 3:420–430. [PubMed: 20176713]

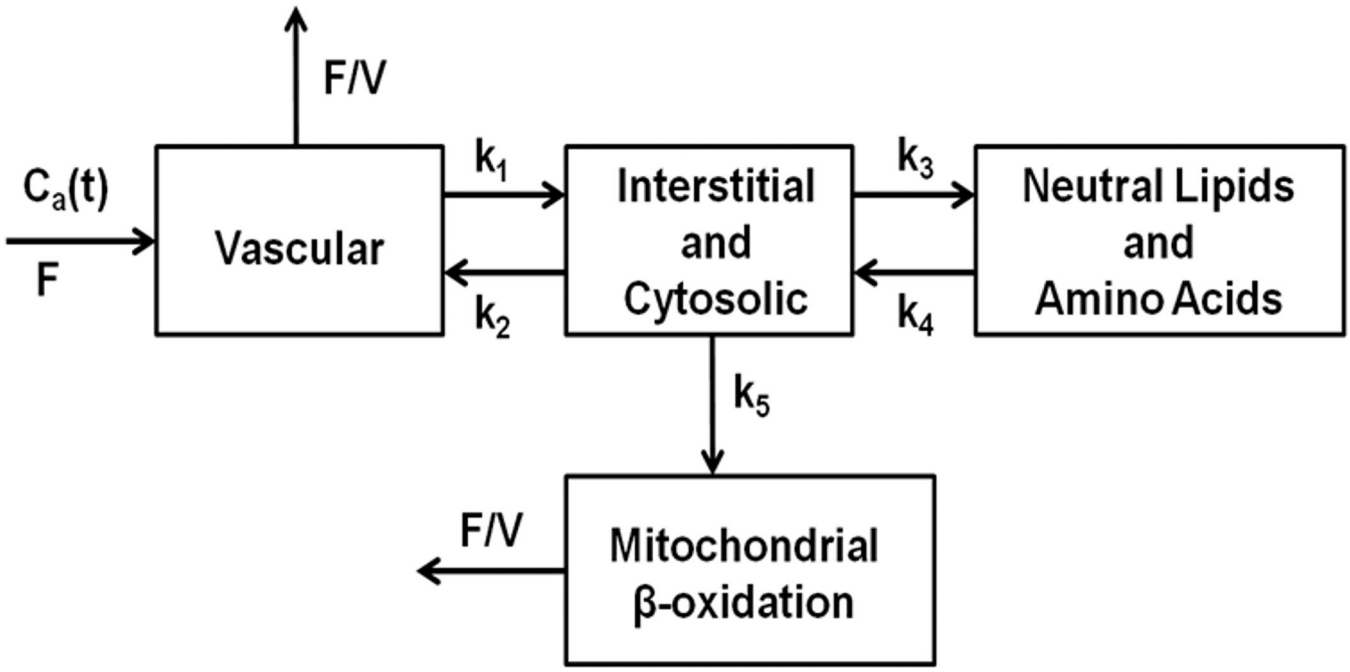

Figure 1. Block diagram of the 4-compartment model

Compartment 1 represents the vascular space; 2, the interstitial and intracellular spaces; 3, neutral lipids, amino acids and other slow turnover pools; and 4, mitochondrial β-oxidation. k_n represents the forward and backward rate constants between compartments, F is myocardial blood flow, V is fractional vascular volume and $C_a(t)$ is arterial tracer concentration over time.

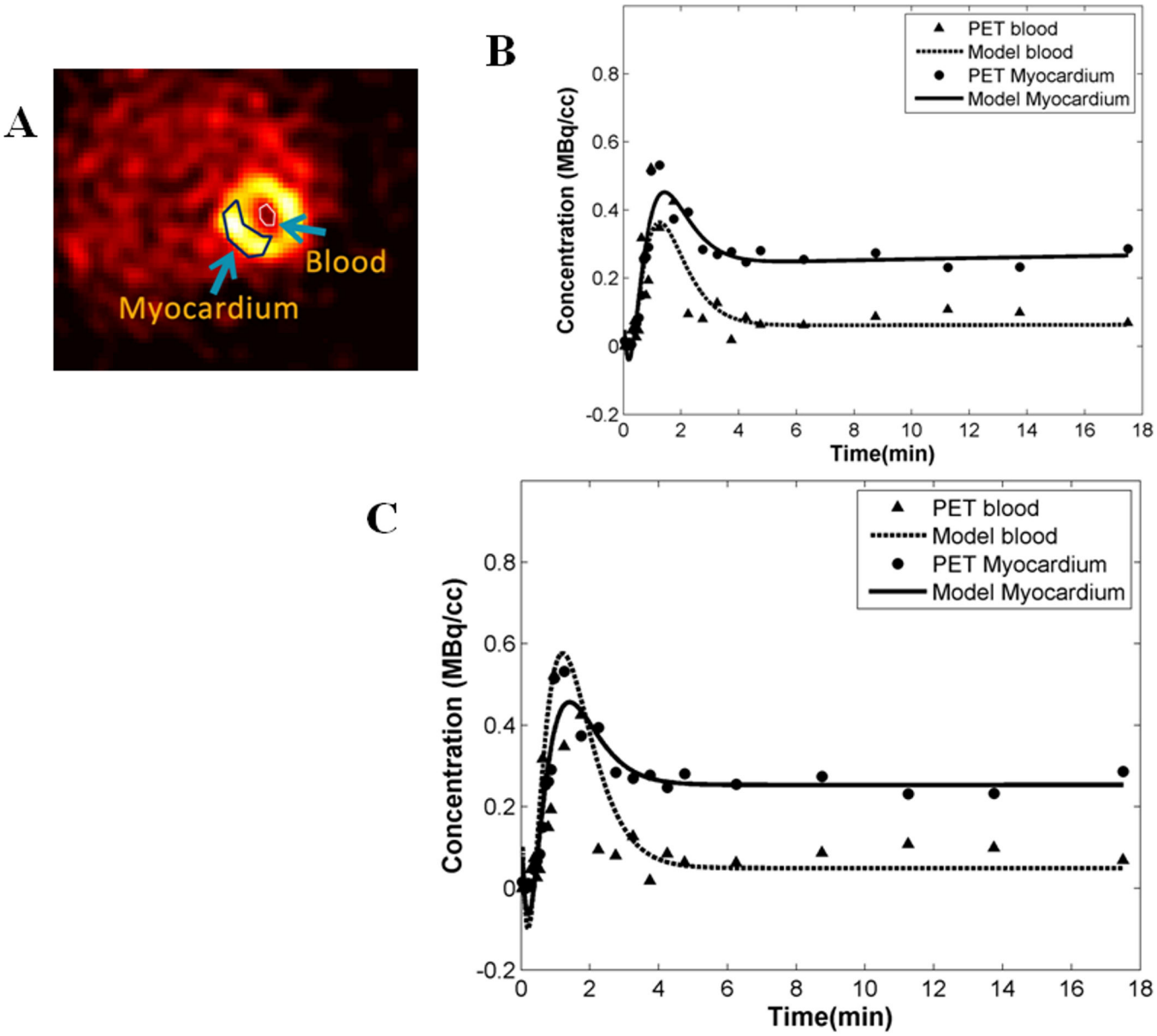

Figure 2. ^{11}**C-palmitate PET images of mouse heart *in vivo***

(A) Example of a PET image at the last time frame of the dynamic data set. The image also exhibits regions of interest in the left ventricular blood pool and the myocardium. **(B)** Model fits to the blood and the myocardial time activity curves without interpolation. **(C)** Cubic spline interpolation resulted in improved fits especially at the peak region for the time activity curve obtained from the LV blood pool.

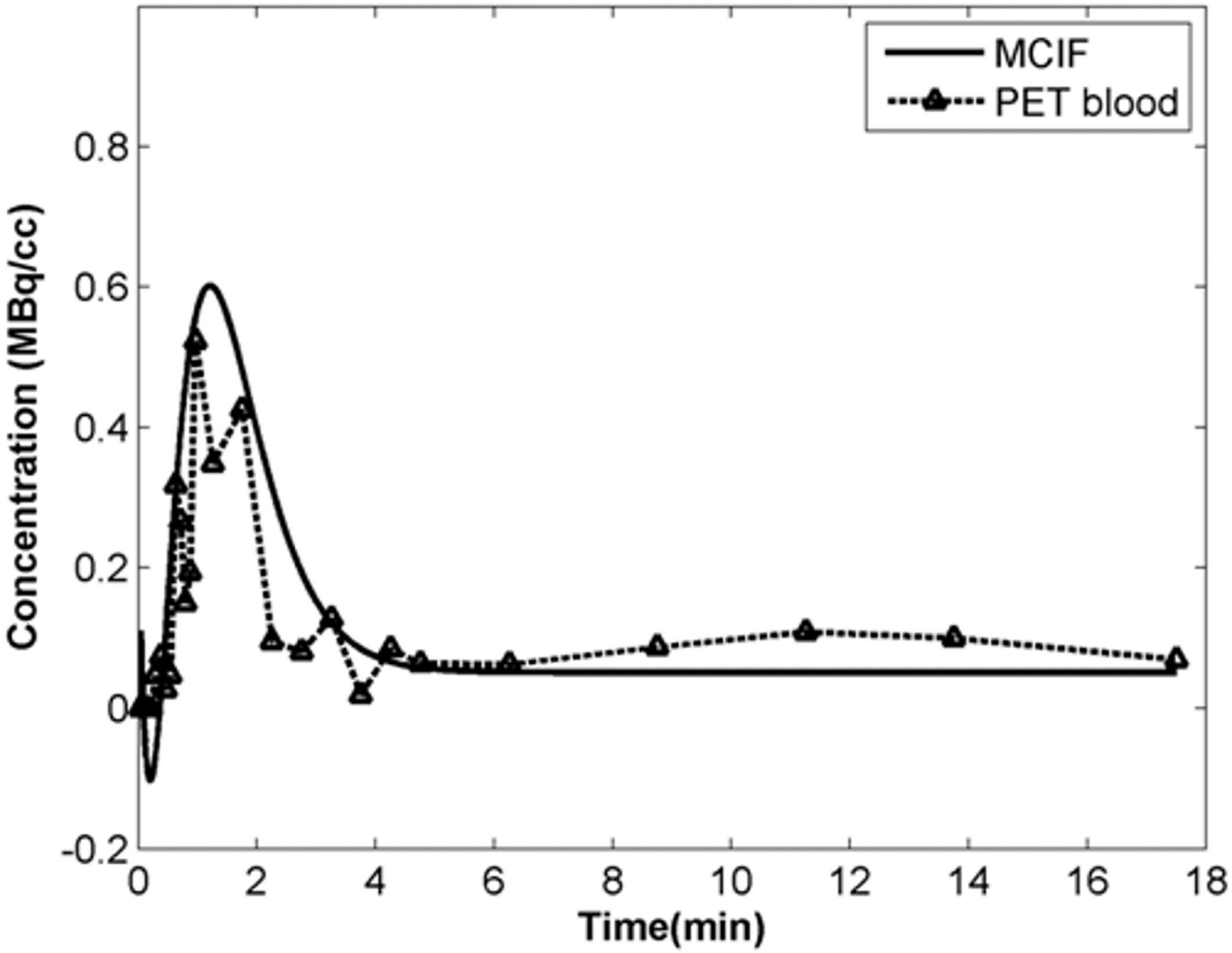

Figure 3. Model corrected blood input function

The model corrected blood input function (MCIF), *Ca(t)*, computed by simultaneous estimation compared to the image-derived blood input function (IDIF: PET blood) obtained from the dynamic ^{11}C-palmitate PET images. MCIF estimation improved radioactivity recovery at the early time points and eliminated SP contamination at the late time points from the myocardium to the LV blood pool.

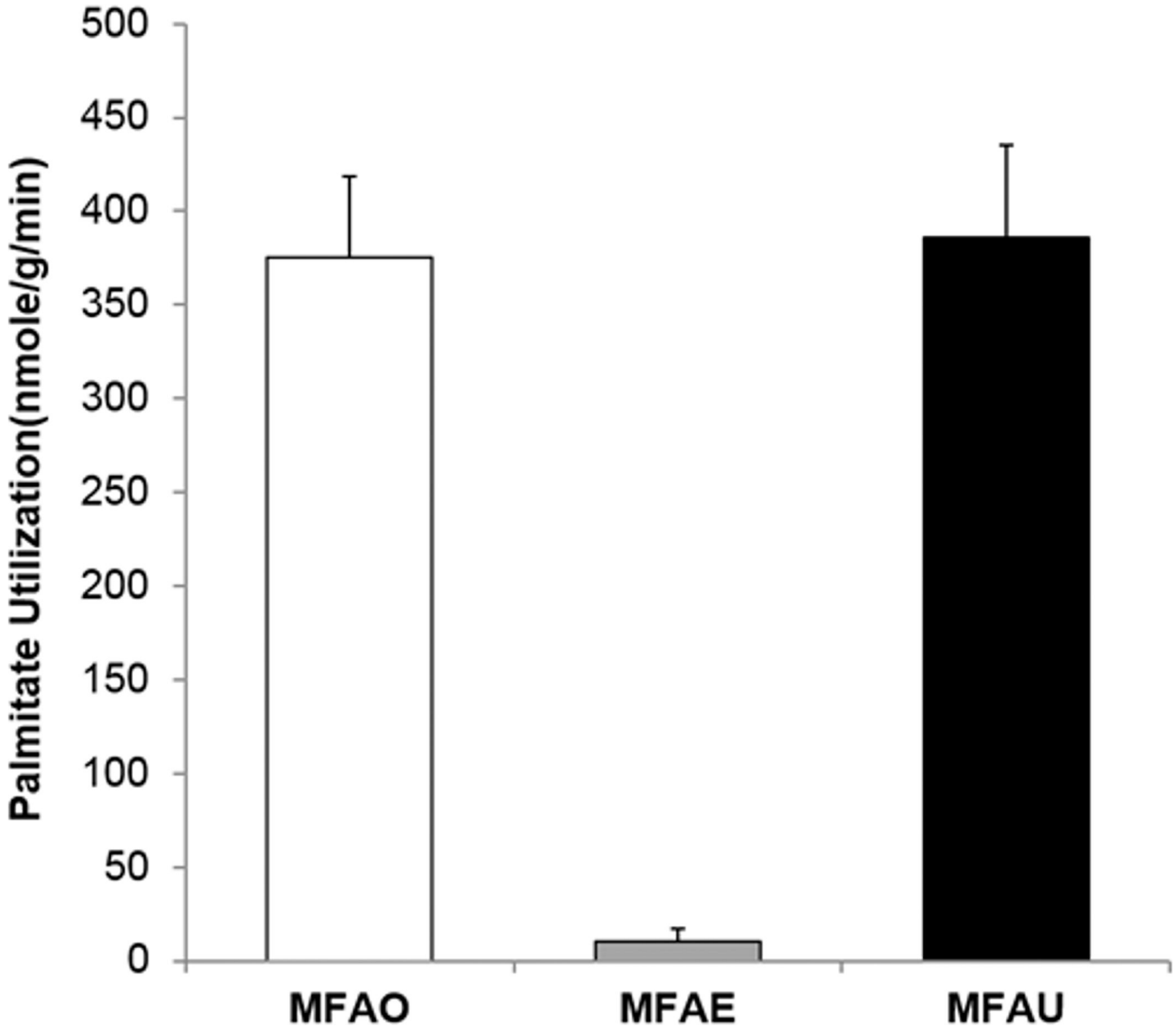

Figure 4. FA metabolic parameters in mouse heart *in vivo*

Myocardial fatty acid oxidation, myocardial fatty acid esterification (MFAE) and myocardial fatty acid utilization (MFAU) computed from dynamic ^{11}C-palmitate PET images of mouse heart *in vivo*.

TABLE 1

Initial Guess Values and Bounds for Parameters Used in the Optimization

Para	k1	k2	k3	k4	k5	Smb	rb	rm	Sbm	A1	A2	A3	L1	L2	L3	tau
Initial	5	0.1	0.1	0.001	0.02	0.01	0.9	0.6	0.5	300	0.1	199.97	−5	−0.06	−1	0.1
Upper	6	1.0	1.0	0.005	1.0	1.0	1.0	0.6	1.0	500	2	500	0	0	0	0.5
Lower	0	0.0	0.0	0.0	0.0	0.0	0.9	0.0	0.4	0	0	0	−10	−1	−10	0

TABLE 2

Optimized rate constants and SP and PV coefficients(n=4)

Number	k1	k2	k3	k4	k5	Smb	rb	rm	Sbm
1	5.9875	0.0079	0.0028	0.0025	0.0596	0.0016	0.9017	0.5989	0.5114
2	4.8115	0.0007	0.0018	0.0025	0.0524	0.0013	0.9569	0.5158	0.6108
3	5.8469	0.0560	0.0008	0.0026	0.1252	0.0012	0.9082	0.5920	0.9863
4	5.9317	0.0055	0.0014	0.0025	0.0567	0.0125	0.9998	0.3688	0.4001
Average	**5.6444**	**0.017525**	**0.0017**	**0.002525**	**0.073475**	**0.00415**	**0.94165**	**0.518875**	**0.62715**
Stdev*	**0.558267**	**0.025824**	**0.000841**	**5E-05**	**0.03461**	**0.005569**	**0.045931**	**0.106901**	**0.254431**

Stdev is the standard deviation.